**Atmospheric
Chemistry
and Physics
Discussions**

Particle mass yield from β-caryophyllene ozonolysis

Q. Chen[1], Y. J. Li[1,2], K. A. McKinney[3], M. Kuwata[1], and S. T. Martin[1,4]

[1]School of Engineering and Applied Sciences, Harvard University, Cambridge, Massachusetts, USA
[2]Division of Environment, Hong Kong University of Science and Technology, Hong Kong, China
[3]Department of Chemistry, Amherst College, Amherst, Massachusetts, USA
[4]Department of Earth and Planetary Sciences, Harvard University, Cambridge, Massachusetts, USA

Correspondence to: S. T. Martin (scot_martin@harvard.edu)

ACPD

11, 30527–30562, 2011

Particle mass yield from β-caryophyllene ozonolysis

Q. Chen et al.

Title Page

Abstract	Introduction
Conclusions	References
Tables	Figures

|◄ | ►|
◄ | ►

Back | Close

Full Screen / Esc

Printer-friendly Version

Interactive Discussion

Abstract

The influence of second-generation products on the particle mass yield of β-caryophyllene ozonolysis was systematically tested and quantified. The approach was to vary the relative concentrations of first- and second-generation products by controlling ozone concentration, while observing the change in particle mass yield. For all organic particle mass concentrations M_{org} of this study ($0.5 < M_{org} < 230\,\mu\mathrm{g\,m}^{-3}$), the data show that particle-phase organic material was in large part composed of second-generation products. For $0.5 < M_{org} < 10\,\mu\mathrm{g\,m}^{-3}$, a range which overlaps with atmospheric concentrations, the particle mass yield was not sensitive to ozone exposure, implying that the constituent molecules were rapidly produced at all investigated ozone exposures. In contrast, for $M_{org} > 10\,\mu\mathrm{g\,m}^{-3}$ the particle mass yield increased with ozone exposure. These different dependencies on ozone exposure with M_{org} are explained by a combination of the ozonolysis lifetimes of the first-generation products and the volatility distribution of the resulting second-generation products. First-generation products that have short lifetimes produce low-volatility second-generation products whereas first-generation products that have long lifetimes produce high-volatility second-generation products. The ultimate particle mass yield was defined by mass-based stoichiometric yields $\alpha_0 = 0.17 \pm 0.05$, $\alpha_1 = 0.11 \pm 0.17$, and $\alpha_2 = 1.03 \pm 0.30$ for corresponding saturation concentrations of 1, 10, and $100\,\mu\mathrm{g\,m}^{-3}$. Terms α_0 and α_1 had low sensitivity to the investigated range of ozone exposure whereas term α_2 increased from 0.32 ± 0.13 to 1.03 ± 0.30 as the ozone exposure was increased. These findings potentially allow for simplified yet nevertheless accurate parameterizations in air quality and climate models that seek to represent the ozonolysis particle mass yield of certain classes of biogenic compounds.

Title Page

Abstract	Introduction
Conclusions	References
Tables	Figures

⏮ ⏭

◀ ▶

Back | Close

Full Screen / Esc

Printer-friendly Version

Interactive Discussion

1 Introduction

Sesquiterpene emissions have been estimated as 10–30 % of those of monoterpenes (Helmig et al., 2007; Sakulyanontvittaya et al., 2008a). Because of their fast ozonolysis reactivity and their tendency to form low-volatility products, sesquiterpenes ($C_{15}H_{24}$)
5 are important precursor molecules to secondary organic material (SOM) (Hoffmann et al., 1997; Jaoui and Kamens, 2003; Jaoui et al., 2003). For instance, β-caryophyllinic acid, which is an ozonolysis product of the sesquiterpene β-caryophyllene, has been measured at substantial concentrations for ambient particles in environments as diverse as the tropics and the arctic (Jaoui et al., 2007; Hu et al., 2008; Fu et al., 2009).
10 For typical concentrations of tropospheric oxidants, the lifetimes of sesquiterpenes are about 2 min for the reaction with ozone, 2–3 min for the reaction with nitrate radicals at night, and 30–40 min for the reaction with hydroxyl radicals in the day (Shu and Atkinson, 1995). Sesquiterpene emissions usually occur during the day (Helmig et al., 2007). Reaction with ozone is therefore regarded as the dominant degradation path-
15 way of many sesquiterpenes in the atmosphere (Atkinson and Arey, 2003).

As one of the most atmospherically prevalent sesquiterpenes, β-caryophyllene has been studied extensively in the laboratory. The reported particle mass yields associated with its oxidation range from 6–62 % for dark ozonolysis and from 37–125 % for photooxidation (Grosjean et al., 1993; Hoffmann et al., 1997; Griffin et al., 1999; Jaoui
20 et al., 2003; Lee et al., 2006a,b; Winterhalter et al., 2009) (Table 1). Particle mass yield Y is defined as the organic particle mass concentration ΔM_{org} that is produced divided by the mass concentration of the precursor volatile organic compound ΔVOC that is reacted (Odum et al., 1996): $Y \equiv \Delta M_{\text{org}}/\Delta \text{VOC}$. Yield depends to a first approximation on the volatility of the reaction products. An implication is that the relative tendency of
25 molecules to partition from the gas phase to the particle phase (i.e., ΔM_{org}) depends on the extent of particle phase (i.e., M_{org}) that is present (Pankow, 1994b,a). Reaction conditions also influence yield by affecting the relative importance of competing kinetic pathways and hence the relative proportion of products of differing volatilities

(Chan et al., 2007). Important experimental conditions include relative humidity, particle acidity, ozone concentration, and NO_x concentration (Ng et al., 2007; Offenberg et al., 2009; Winterhalter et al., 2009). Winterhalter et al. (2009), for example, demonstrated that the addition of gas-phase formic acid or water scavenged reactive Criegee intermediates and thereby influenced the concentration profile of the reaction products, ultimately leading to a doubling of the particle mass yield by β-caryophyllene ozonolysis. Offenberg et al. (2009) showed that increased particle acidity led to greater particle mass yields from β-caryophyllene photooxidation.

Among the several factors influencing particle mass yield from β-caryophyllene ozonolysis, the stoichiometric ratio of ozone to β-caryophyllene is an especially important regulator. β-caryophyllene has two double bonds, and the endocyclic bond is more reactive to ozone by two orders of magnitude than is the exocyclic bond (Nguyen et al., 2009; Winterhalter et al., 2009). Second-generation products are produced by ozonolysis of the remaining double bond of the first-generation products. The second-generation products typically have lower vapor pressures and hence greater thermodynamic tendencies to condense to the particle phase (Li et al., 2011). As a result, particle mass yield increases significantly in the case that sufficient ozone is present for first-generation products to continue oxidation. For instance, when injecting excess ozone, Ng et al. (2006) observed continued and rapid particle growth even after β-caryophyllene was completely consumed. This observation was explained by the production and gas-to-particle condensation of second-generation products.

In the atmosphere, concentrations of biogenic volatile organic compounds (BVOCs) are ultimately limited by their surface emissions and are normally less than 10 ppbv in forested environments (Helmig et al., 1998). By comparison, ozone concentrations range from 10 to 30 ppbv at background sites (Fiore et al., 2003) to over 100 ppbv for urban locations (Solomon et al., 2000). Moreover, the atmospheric concentration of ozone is continuously renewed by atmospheric production. The implication is that under most circumstances the ozone concentration is in excess of the possible consumption by BVOCs, especially for sesquiterpenes. Few laboratory studies, however, have

carried out experiments for conditions of excess ozone (i.e., ozone : β-caryophyllene > 2) (Table 1). As such, particle mass yield in the regime of second-generation dominance remains largely unknown, especially for conditions that overlap with atmospheric concentrations ($M_{org} < 10\,\mu g\,m^{-3}$).

5   Herein, experimental observations for the dark ozonolysis of β-caryophyllene (0.8–46 ppbv) under various conditions of excess ozone are reported. The qualitative molecular identification of the particle-phase products for these experiments and an associated discussion of their production mechanisms were presented in Li et al. (2011). An analysis of oxygen-to-carbon (O:C) and hydrogen-to-carbon (H:C) elemental ratios

10 was presented in Chen et al. (2011) in a comparative study of isoprene, α-pinene, and β-caryophyllene. In relation to these two earlier reports, the focus of the present report is on second-generation products and their effects on particle mass yield.

2 Experimental

2.1 Experimental procedures and measurements

15 Experiments were carried out in the Harvard Environmental Chamber. Detailed descriptions of the chamber were previously published (Shilling et al., 2008; King et al., 2009). Compared to those reports, in this study a 0.13-mm (5-mil) thick PFA Teflon bag having a volume V of $4.7\,m^3$ was newly installed as a replacement for the previously described 0.05-mm (2-mil) PFA bag. As in the earlier studies, the bag served as a con-

20 tinuously mixed flow reactor (CMFR) (Kleindienst et al., 1999; Seinfeld et al., 2003). A flow Q of $22\,l\,min^{-1}$ was used, corresponding to a mean residence time τ of 3.6 h, as calculated by $\tau = V/Q$. Temperature and relative humidity were held at $25 \pm 1\,°C$ and $40 \pm 1\,\%$, respectively.

    Ammonium sulfate particles were continuously present in the inflow of the CMFR.

25 The surfaces of these particles served as a suspended substrate to accommodate the gas-to-particle condensation of the oxidation products of β-caryophyllene. An

ammonium sulfate solution (Sigma-Aldrich, ≥ 99.0 %) was atomized (TSI, 3076, Liu and Lee, 1975) to produce a polydisperse particle population, which was then dried in a 160-cm silica gel diffusion dryer (RH < 10 %). A monodisperse electric-mobility fraction was selected from the population by a differential mobility analyzer (TSI, 3071 DMA; [85]Kr bipolar charger) (Knutson and Whitby, 1975). The DMA was operated with $10\,l\,min^{-1}$ sheath and $2\,l\,min^{-1}$ aerosol flows. Electric-equivalent (+1 charge) mobility diameters $d_{m,+1}$ of the seed particles for each experiment are summarized in Table 2. The corresponding surface area concentration inside the CMFR prior to initiating β-caryophyllene ozonolysis was $(4.0 \pm 2.0) \times 10^{-5}\,m^2\,m^{-3}$. For experiments at the highest initial β-caryophyllene concentration of 46.4 ppbv, polydisperse seed particles were used instead of monodisperse ones so that the surface area concentration $(2.0 \times 10^{-3}\,m^2\,m^{-3})$ was sufficiently high to minimize the contribution of particles formed by homogeneous nucleation of the organic gases.

In a series of experiments, the initial concentration of β-caryophyllene inside the CMFR prior to ozonolysis was varied from 0.8 to 46.4 ppbv. A liquid solution (1 : 2500, v/v) of β-caryophyllene (Sigma-Aldrich, ≥ 98.5 %) in cyclohexane (Sigma-Aldrich, ≥ 99.9 %) was fed by a syringe pump into a round-bottom flask warmed to 70 °C. A continuous flow of air swept the evaporated molecules of β-caryophyllene and cyclohexane from the flask into the CMFR for the entire experimental period. The concentration of β-caryophyllene inside the CMFR was adjusted by using a variable rate of liquid injection from the syringe pump. Cyclohexane served as a scavenger of hydroxyl radicals produced by some ozonolysis pathways. A quadrupole proton-transfer-reaction mass spectrometer (Ionicon, PTR-MS) was used both to confirm the β-caryophyllene concentration in the CMFR prior to ozone injection and to track the extent of reaction after ozone injection (Shilling et al., 2008). Ozone concentrations of 50, 100, and 200 ppbv were used during the conducted experiments (Table 2). Within a single experiment, the ozone concentration was held constant by feedback control, meaning that sufficient ozone was added to react away nearly all the β-caryophyllene while maintaining a constant concentration of 50, 100, or 200 ppbv. For all experiments (Table 2), the

Title Page

Abstract	Introduction
Conclusions	References
Tables	Figures

|◄| |►|
|◄| |►|

| Back | Close |

Full Screen / Esc

Printer-friendly Version

Interactive Discussion

ozone concentrations were therefore in excess compared to the reacted concentrations of β-caryophyllene.

The outflow of the CMFR was continuously sampled by a scanning mobility particle sizer (TSI, 3936 L22 SMPS, Wang and Flagan, 1989), filter-based collection for off-line molecular analysis by an ultra-performance liquid chromatography coupled to an electrospray-ionization time-of-flight mass spectrometer (Waters, ACQUITY/LCT Premier XE UPLC-ESI-ToF-MS, Neue et al., 2010), and an on-line particle-vaporization electron-impact high-resolution time-of-flight mass spectrometer (Aerodyne, HR-ToF-AMS, DeCarlo et al., 2006). The SMPS provided measurements of the number-diameter distribution of the particle population. The UPLC-ESI-ToF-MS molecular analysis of the material sampled onto the filters was previously presented in Li et al. (2011). The HR-ToF-AMS was used for the in situ collection of the mass spectrum of the particle population in the CMFR outflow. At steady state of a single experiment, no significant changes in the mass spectra were observed, and the AMS data sets were averaged for 4 to 12 h for each steady-state condition to increase the signal-to-noise ratio. For experiment #27 (Table 2), a DMA (TSI, 3071; ^{85}Kr bipolar charger) was coupled to an aerosol particle mass analyzer (Kanomax, APM 3600, Ehara et al., 1996) to measure the particle effective density.

The CMFR is an experimental configuration that can facilitate the study of ultimate yield by providing a mean residence time sufficient for multi-generational chemistry (Kleindienst et al., 1999). For example, the average ozonolysis lifetime of the first-generation products of β-caryophyllene is about 0.5 h (1860 s) at 200 ppbv ozone based on a rate constant of $(1.1 \pm 0.4) \times 10^{-16}$ molecule^{-1} cm^3 s^{-1} and the lifetime of β-caryophyllene is 20 s based on a rate constant of $(1.2 \pm 0.1) \times 10^{-14}$ molecule^{-1} cm^3 s^{-1} (Shu and Atkinson, 1995; Winterhalter et al., 2009). In comparison, the mean residence time of the Harvard Environmental Chamber for most experiments is 3.6 h (13 100 s) (Shilling et al., 2008; King et al., 2009). The CMFR operation can also improve the precision and accuracy of yield measurement at low M_{org} by providing sufficient observation time for significant signal averaging (Shilling et al., 2008). Unlike the

ozonolysis of monoterpenes, the particle mass yield from β-caryophyllene ozonolysis under ozone-excess conditions cannot be derived from progressive measurements of ΔVOC and ΔM_{org} in a single static chamber experiment (Presto and Donahue, 2006) because the time-dependent data do not represent the ultimate particle growth for a given amount of reacted hydrocarbon (Ng et al., 2006).

2.2 AMS data analysis

The spectra collected by the AMS were used to calculate the mass concentrations and the elemental ratios of the particle-phase secondary organic material present in the outflow from the CMFR (Table 2). The spectra were analyzed using the software toolkits *Sequential Igor Data Retrieval* (SQUIRREL), *Peak Integration by Key Analysis* (PIKA), and *Analytic Procedure for Elemental Separation* (APES) (DeCarlo et al., 2006; Aiken et al., 2007). In the analysis, standard relative ionization efficiencies (RIE) were used, corresponding to 1.1 for nitrate, 1.2 for sulfate, 1.4 for organic molecules, 4.0 for ammonium, 1.3 for chloride, and 2.0 for water (Alfarra et al., 2004; Mensah et al., 2011). An AMS collection efficiency (a factor which potentially corrects for undetected particle mass concentration) of 1.0 was used, as supported by the agreement of the AMS-measured mass concentrations with the density-compensated volume concentrations measured by the SMPS (Sect. 2.3). Determination of the air correction factors, several updates to the fragmentation table, and the contributions of organic material to CO^+ and H_xO^+ signal intensities followed the method described in Chen et al. (2011).

2.3 Material density

Under an assumption of spherical particles, volume-diameter distributions measured by the SMPS can be used in conjunction with mass-diameter distributions measured by the AMS to estimate the particle effective density ρ_{eff} (kg m^{-3}). More specifically, ρ_{eff} was calculated by dividing the mass-mode particle diameter measured by the AMS (i.e., vacuum aerodynamic diameter) by the volume-mode diameter measured by the

SMPS (i.e., mobility diameter) (DeCarlo et al., 2004; Bahreini et al., 2005; Katrib et al., 2005). Figure S1 shows two examples of the mass-diameter distribution derived from the SMPS measurements compared to that measured by the AMS for particles in the CMFR outflow. The SMPS mass-diameter distributions were derived by multiplying the SMPS volume-diameter distributions by ρ_{eff} (i.e., obtained using the mode diameters). The good agreement between the SMPS and AMS distributions suggests that, within detection limits, ρ_{eff} does not vary with diameter. The integrated area under the distributions represents the total particle mass concentration. Figure S2 shows the scatter plot of the total mass concentrations obtained from the AMS measurements against the SMPS-derived concentrations. The slope of 0.99 ± 0.02 indicates that an AMS collection efficiency of unity can be assumed given the measurement uncertainties of the AMS and the SMPS (Matthew et al., 2008).

For nonporous spherical particles, effective density reduces to material density (De-Carlo et al., 2004). Past work indicates the applicability of a nonporous spherical morphology for SOM-coated sulfate particles (King et al., 2007). Based on the ρ_{eff} value obtained for each experiment, the material density ρ_{org} of the SOM was calculated by the rule of volume additivity. As explained by Bahreini et al. (2005) for AMS data, this rule states that $\rho_{org} = M_{org}/(M_{particle}/\rho_{eff} - M_{AS}/\rho_{AS})$, where ρ_{AS} is the material density of ammonium sulfate ($1770 \, \text{kg m}^{-3}$), $M_{particle}$ is the total particle mass concentration ($\mu\text{g m}^{-3}$), and M_{AS} is the ammonium sulfate mass concentration ($\mu\text{g m}^{-3}$). The presented equation is valid provided that the chemical components either do not mix or alternatively have a numerically small excess volume of mixing. The ρ_{org} values obtained by this analysis and their uncertainties are listed in Table 2. The uncertainties of 5 to 10 % were derived by the Monte Carlo method. Input parameters for this analysis were the size resolutions of the instruments and the standard deviations of the temporal variation of the measured quantities.

For experiment #27 (Table 2), independent measurements of ρ_{eff} and hence independent calculations of ρ_{org} were also made by the DMA-APM methodology (Kuwata et al., 2011). In this case, ρ_{org} was calculated from data of quasi-monodisperse

Title Page

Abstract | Introduction

Conclusions | References

Tables | Figures

◄ | ►|

◄ | ►

Back | Close

Full Screen / Esc

Printer-friendly Version

Interactive Discussion

particles rather than for the entire particle population. The uncertainty of ρ_{org} for the DMA-APM method was estimated as 2 % on the basis of calibrations using polystyrene latex particles.

Figure S3 shows that the ρ_{org} values determined by the independent AMS-SMPS and DMA-APM methods were in agreement. The measured value of ρ_{org} of $1320 \pm 20\,\text{kg m}^{-3}$ at high mass concentrations ($M_{\text{org}} > 50\,\mu\text{g m}^{-3}$) was also consistent with the value reported previously by Bahreini et al. (2005) for β-caryophyllene ozonolysis for M_{org} of $300\,\mu\text{g m}^{-3}$. Figure S3 also shows that there was a dependence of ρ_{org} on organic particle mass concentration. A similar result was reported previously for α-pinene ozonolysis (Shilling et al., 2009).

2.4 Particle mass yield

Particle mass yield Y is defined as $Y \equiv \Delta M_{\text{org}}/\Delta\text{VOC}$, with the sign construed as positive. The term ΔVOC is the difference in the β-caryophyllene concentration between the outflow and the inflow of the CMFR, meaning that negligible loss is assumed for unreacted β-caryophyllene to any apparatus surfaces. The accuracy of this assumption was supported by the agreement between the β-caryophyllene concentrations in the CMFR outflow prior to initiation of reaction (as measured by the PTR-MS) and the concentrations calculated from the liquid injection rate from the syringe pump and the subsequent dilution with air flows.

For ΔM_{org}, a simplification is that the inflow concentration is zero but a complication is that significant mass is lost to the walls of the bag and therefore does not contribute to concentration measured in the outflow. Therefore, $\Delta M_{\text{org}} = (M_{\text{org}})_{\text{outflow}} + (M_{\text{org}})_{\text{wallloss}} - (M_{\text{org}})_{\text{inflow}}$. We measure $(M_{\text{org}})_{\text{outflow}}$ using the AMS, we know $(M_{\text{org}})_{\text{inflow}} = 0$, and we relate $(M_{\text{org}})_{\text{wallloss}} = f\left((M_{\text{org}})_{\text{outflow}}\right)$ by calibration of wall loss rates. More specifically, $(M_{\text{org}})_{\text{wallloss}} = \beta\tau(M_{\text{org}})_{\text{outflow}}$ for an assumed first-order diameter-independent particle wall-loss coefficient β (s^{-1}) and a mean residence time τ (s) in the CMFR (Seinfeld et al., 2003; Pierce et al., 2008). Wall-loss mechanisms include Brownian diffusion,

electrostatic forces, and gravitational sedimentation (McMurry and Grosjean, 1985).

The final form of equation for particle mass yield for the conducted experiments is as follows:

$$Y = \left| \frac{(1 + \beta\tau)(M_{org})_{outflow}}{VOC_{outflow} - VOC_{inflow}} \right| \tag{1}$$

For further use, we also introduce here the definition $M_{org,corr} \equiv (1 + \beta\tau)(M_{org})_{outflow}$ as the wall-loss corrected organic particle mass concentration.

The particle wall-loss coefficient β can be determined experimentally by measuring the change in number concentration of surrogate particles in the chamber (McMurry and Grosjean, 1985). For this purpose, experiments were conducted with populations of ammonium sulfate particles in the absence of organic material. On the basis of the particle number balance in the CMFR (Seinfeld et al., 2003), $\beta = (2.9 \pm 0.3) \times 10^{-4}\,s^{-1}$ was obtained, and no significant dependence of β on diameter was observed for the studied populations (Fig. 1). For number-diameter distributions of SOM-coated sulfate particles of the actual experiments (Fig. S4), independent estimates of $\beta = (2.8 \pm 0.4) \times 10^{-4}\,s^{-1}$ were obtained by comparing the total particle number concentrations measured in the CMFR outflow to the total concentrations expected based on the seed particle concentrations in the CMFR inflow.

The measured wall-loss coefficients of the present study were greater than the measured values for the earlier experiments in the Harvard Environmental Chamber. Shilling et al. (2008) reported $\beta = 4.7$ to $2.5 \times 10^{-5}\,s^{-1}$ for dry ammonium sulfate particles of 50 to 150 nm. The explanation for the difference is the use of an aged bag in the study of Shilling et al. (2008) and a new Teflon bag for most experiments of the present study. In support of this explanation, the experiments described herein from April to June 2009 produced the reported β values, and no systematic temporal trend of wall losses was observed during this time period, suggesting that the effects of bag aging during the two months of experiments were minimal. In September 2010, with the by-then aged bag, β values in agreement with Shilling et al. (2008) were obtained,

as represented by experiment #27 of Table 2. The additional aging of the bag surface significantly decreased the particle wall losses, perhaps because of surface alterations that influenced electrostatic charging (McMurry and Rader, 1985). In support of this explanation, re-neutralization of the seed particles prior to the injection decreased par-
5 ticle wall losses, as represented by experiment #10 of Table 2.

The particle-phase organic mass concentrations were corrected by 68 to 370 % for the different β values of the experiments (Eq. 1). The corrected values were in agreement within uncertainty (Fig. S5), supporting the accuracy of the applied corrections. Experiments carried out at repeated conditions support the reproducibility of the results
10 (Table 2).

3   Results and discussion

Figure 2 shows a typical time series for the transient period prior to steady-state in the CMFR. The time traces show the loss of β-caryophyllene after the introduction of ozone and the appearance of particle-phase secondary organic material. Seed particles and
15 β-caryophyllene were introduced into the CMFR and reached steady-state concentrations prior to the injection of ozone. Once ozone was introduced, the concentration of β-caryophyllene decreased rapidly. After a transient period, the feedback circuit between the measured ozone concentration and the quantity of ozone injected into the bag successfully maintained the ozone concentration at 50 ppbv. The steady-state
20 concentrations of particle-phase SOM were reached after 8 h and were maintained until completion of the experiment after 56 h.

During the transient period of Fig. 2, the initial consumption of β-caryophyllene was primarily by the reaction of ozone with the endo-cyclic double bond. The ozonolysis rate constant of the endo-cyclic double bond of β-caryophyllene ($k_{endo} =$
25 1.16×10^{-14} molecule^{-1} cm^3 s^{-1}) is 100× greater than that of the exo-cyclic double bond of the first-generation products ($k_{exo} = 1.1 \times 10^{-16}$ molecule^{-1} cm^3 s^{-1}) (Shu and Atkinson, 1995; Winterhalter et al., 2009). The time decay of the β-caryophyllene

Particle mass yield from β-caryophyllene ozonolysis

Q. Chen et al.

Title Page

Abstract	Introduction
Conclusions	References
Tables	Figures

|◄ | ►|

| ◄ | ► |

| Back | Close |

Full Screen / Esc

Printer-friendly Version

Interactive Discussion

concentration agreed well with that predicted for the CMFR (i.e., the modeled line in Fig. 2) using the rate constant k_{endo} and the measured ozone concentrations.

Subsequent to the first transient period, Fig. 2 shows that a further increase in the ozone concentration to 200 ppbv causes an increase in the mass concentration of particle-phase SOM. The remaining exo-cyclic double bond of the first-generation products may react at the higher ozone concentration, leading to additional low-volatility products that partition to the particle phase (Kanawati et al., 2008; Li et al., 2011). The data of Fig. 3 demonstrate the generalization of this result, showing an increase in yield for 200 compared to 50 ppbv ozone for all experiments of this study.

The representation in Fig. 2 can be put into a quantitative context by comparing the ozone-dependent e-folding lifetimes $\tau_{endo}(O_3)$ and $\tau_{exo}(O_3)$ of the two double bonds at 50 and 200 ppbv (i.e., $\tau(O_3)=1/k[O_3]$) to the mean CMFR residence time τ_{CMFR}. The values are as follows: $\tau_{endo}(50) = 70$ s, $\tau_{endo}(200) = 20$ s, $\tau_{exo}(50) = 7500$ s, $\tau_{exo}(200) = 2000$ s, and $\tau_{CMFR} = 13\,100$ s. The relationships $\tau_{CMFR}/\tau_{endo}(50) \gg 10$ and $\tau_{CMFR}/\tau_{endo}(200) \gg 10$ imply that β-caryophyllene is consumed nearly 100 % for both ozone concentrations. This result is supported by the PTR-MS measurements show a negligible residual β-caryophyllene concentration in the CMFR outflow for 50 and 200 ppbv ozone (Fig. 2).

The population of first-generation products i has a distribution of reactivity $\tau_{exo,i}$ with respect to ozonolysis of the remaining exo-cyclic double bond. This distribution in reactivity is assumed to be represented by a mean value τ_{exo} and an associated variance σ^2 for the population of products. The calculations $\tau_{CMFR}/\tau_{exo}(50) = 1.8$ and $\tau_{CMFR}/\tau_{exo}(50) = 6.6$ suggest that for many products i the relationships $0.1 < \tau_{CMFR}/\tau_{exo,i}(50) < 10$ and $0.1 < \tau_{CMFR}/\tau_{exo,i}(200) < 10$ hold, implying that there are significant differences among the various first-generation products in the timescales for conversion from first- to second-generation products. These differences are sensitive to the ozone concentration in the CMFR. For instance, a kinetics calculation (cf. Sect. A of Supplement) suggests a mean conversion of 63 % from first- to second-generation products for 50 ppbv ozone compared to a mean conversion of 87 % for

Full Screen / Esc

Printer-friendly Version

Interactive Discussion

200 ppbv ozone. The actual overall conversion to second-generation products depends upon the unknown probability density function PDF(τ_{exo}, σ) of reactant concentrations and reactivity. The experimental observations of Fig. 2 show that there is a 60 % increase in $(M_{org})_{outflow}$ for 200 compared to 50 ppbv ozone. This increase is caused by the additional conversion of first- to second-generation products at 200 ppbv ozone.

Differences in particle-phase molecular products between 50 and 200 ppbv ozone exposure, as highlighted in Fig. 4, are consistent with an enhancement of second-generation products relative to first-generation ones. Figure 4a shows the ozone-dependent mass fractions of first- compared to second-generation products, as determined by UPLC-ESI-ToF-MS for 15 compounds (Li et al., 2011). As the ozone concentration increases, the second-generation products are increasingly dominant.

Figure 4b shows the percent change in mass concentration for exposure to 50 compared to 200 ppbv ozone for each of the 15 products. The structures of the products labeled in Fig. 4 are provided in Li et al. (2011) and are reproduced for convenience in Fig. S6. Figure 4b shows that the mass concentrations of the first-generation products decrease and the concentrations of the second-generation products increase at higher ozone concentration, as is consistent with the conversion of the former into the latter. The concentration of P270-1 represents the largest relative change, suggesting that its first-generation precursor compound has a relatively low ozonolysis rate constant. There are, however, a few exceptions apparent to this trend. Unlike other second-generation products, the mass concentrations of the products P252-4 and P302 do not change, suggesting that at 50 ppbv ozone they are already produced to completion from their first-generation precursors. Another exception is P238, showing a negative relative change in mass concentration. This species is produced by an ozone channel that competes with an RO_2 channel (cf. Fig. S6), and the RO_2 channel leading to P198 may be more predominant at higher ozone concentration.

Unlike other first-generation products, the mass concentrations of the products P252-x and P254-1 increase at 200 ppbv ozone. The relative concentration change of P252-x is within the uncertainty, which is consistent with the nearly completion of P302

from P252-1 at 50 ppbv ozone. P254-1 was assigned previously as the first-generation product β-caryophyllinic acid, which has been observed in ambient samples and used as a tracer for β-caryophyllene SOM (Jaoui et al., 2007; Kleindienst et al., 2007; Hu et al., 2008). A second-generation product (β-nocaryophyllonic acid), however, has the same exact mass at P254-1 (Jaoui et al., 2003; Chan et al., 2011). Our data are consistent with the plausible suggestion that P254-1 has been incorrectly assigned as β-caryophyllinic acid by Li et al. (2011) and that it should instead be assigned as the second-generation product β-nocaryophyllonic acid.

Figure 5 presents the yield data for increasing organic particle mass concentration. Yield data are customarily parameterized with the objective of further upscale modeling (e.g., air quality models). In common usage, parameterizations are based on either a two-product model (Odum et al., 1996) or a basis-set approach (Presto and Donahue, 2006). Our application employs the latter. The products formed by the oxidation of β-caryophyllene are binned into product classes of mass yields α_i, and the volatilities of the product classes are prescribed in decadal units of 10^{-i}, where 10^{-i} is denoted as C_i^*. Particle mass yield is then written (Seinfeld and Pankow, 2003; Presto and Donahue, 2006):

$$Y(M_{\text{org,corr}}) \equiv \frac{\Delta M_{\text{org}}}{\Delta \text{VOC}} = \sum_{i=i_i}^{i_f} \alpha_i \left(1 + \frac{C_i^*}{M_{\text{org,corr}}}\right)^{-1} \tag{2}$$

The yield data sets in panels a1–a3, which represent the three different ozone concentrations of this study, were each fit using Eq. (2) for $i_i = 0$ and $i_f = 2$. The fit treated C_i^* (μg m^{-3}) as fixed quantities, Y and $M_{\text{org,corr}}$ as data, and α_i as the quantities for optimization. The overall bar height in panels a1–a3 represents the cumulative potential yield (i.e., $\sum_{i=i_i}^{i_f} \alpha_i$). The coloring inside each bar represents the partitioning of the organic molecules between the gas (gray) and particle (green) phases (Donahue et al., 2006; Presto and Donahue, 2006). The different shades of green represent the volatility associated with a component of the particle phase. The optimized values for

α_i (Table S1) are plotted in the panels b1–b3 for each ozone concentration.

An approximate upper limit of 150 % for the maximum potential particle mass yield from β-caryophyllene ozonolysis can be established by assuming that two ozone molecules add to the original molecule and that all product molecules partition to the particle phase. The representation in panel a1 of Fig. 5 shows that the cumulative yield approaches 60 % for 50 ppbv ozone. By comparison, panel a3 for 200 ppbv ozone shows that the cumulative yield approaches 130 %, suggesting that the overall reaction is nearly complete. The implication is that the particle-phase mass yield represented by each green bar in panel a3 can be taken as the approximate representation of the ultimate yield.

From 50 to 200 ppbv ozone, the optimized mass yields α_i have similar values for products of low volatility ($C_i^* = 1$, $10\,\mu g\,m^{-3}$) but a trend of increasing values for products of relatively high volatility ($C_i^* = 100\,\mu g\,m^{-3}$) (panels b1–b3 of Fig. 5). The similar values of mass yields suggest that the low-volatility products are mainly second-generation products that are formed nearly to completion from their first-generation precursors even at 50 ppbv, indicating fast formation pathways. In this case, the mass yields are not sensitive to the ozone concentration. This conclusion is supported by the molecular data that show a negligible change in the mass concentration of P302 for 50 compared to 200 ppbv ozone; P302 is the product having the lowest volatility among the 15 identified products (Li et al., 2011). Although the molecular data also show that another low-volatility second-generation product P270-1 has the largest increase in mass concentration at 200 ppbv ozone, this product may have a low individual mass yield and hence minimal influence on the overall yield α_i. By comparison, the trend of increasing α_i values with increasing ozone concentration for $C_i^* = 100\,\mu g\,m^{-3}$ suggests that the relatively high-volatility products are mainly second-generation products that are formed by relatively slow pathways. The increase of ozone concentration leads to greater conversion of these products from their first-generation precursors. Panels a1–a3 show the consequence of these processes: the increase in particle mass yield from 50 to 200 ppbv ozone is dominantly driven by products of relatively high volatility

Title Page

Abstract | Introduction

Conclusions | References

Tables | Figures

⏮ | ⏭

◀ | ▶

Back | Close

Full Screen / Esc

Printer-friendly Version

Interactive Discussion

(cf. large light-green bar in panel a3 for $C_i^* = 100\,\mu g\,m^{-3}$).

The findings for α_i represented in panels b1–b3 provide a formal framework for the observation that differences in particle mass yield for 200 ppbv compared to 50 ppbv ozone are small for $M_{org,corr} < 10\,\mu g\,m^{-3}$ but greater for higher $M_{org,corr}$ (panels a1–a3).

⁵ For low $M_{org,corr}$, the particle-phase SOM is dominantly composed of products having low volatility. Therefore, the significantly increased production at 200 ppbv ozone of the high-volatility products of $C_i^* = 100\,\mu g\,m^{-3}$ causes little additional partitioning to the particle phase. By comparison, for $10 \leq M_{org,corr} \leq 100\,\mu g\,m^{-3}$ products of $C_i^* = 100\,\mu g\,m^{-3}$ increasingly partition to the particle phase, meaning that 10 % of these

¹⁰ products partition to the particle phase for $M_{org,corr} = 10\,\mu g\,m^{-3}$ and 50 % of them to the particle phase for $M_{org,corr} = 100\,\mu g\,m^{-3}$ (Donahue et al., 2006).

There is a dependency of the O : C elemental ratio, as measured by the AMS, on $M_{org,corr}$, and this dependency may also be explained by the volatility distribution of the products. The O : C ratios ranges from 0.5 to 0.3 (Table 2), corresponding to an average

¹⁵ addition of 5 to 8 oxygen atoms to the C_{15} structure of β-caryophyllene. This average is consistent with a dominant presence of second-generation products in the particle phase because the first-generation products have from 1 to 4 oxygen atoms (Winter-halter et al., 2009; Li et al., 2011). The experimental results for $M_{org,corr} < 10\,\mu g\,m^{-3}$ show that as ΔVOC (Fig. 6a) and/or steady-state O_3 concentration (Fig. 6b) increases

²⁰ the O : C ratio does not change, at least within measurement uncertainty. This behav-ior is consistent with the dominant contribution of low-volatility, fast-forming second-generation products to the particle phase. By comparison, for $M_{org,corr} > 10\,\mu g\,m^{-3}$ the O : C ratio steadily decreases for increasing ΔVOC and/or ozone concentration. This correspondence between decreased O : C ratio and increased contribution of high-

²⁵ volatility products (i.e., $C_i^* = 100\,\mu g\,m^{-3}$) conforms to the expected structure-function relationship between a molecule's oxygen content and its vapor pressure, meaning greater oxygen content of a molecule and an associated decreased vapor pressure (Pankow and Asher, 2008).

The yield data of this study are summarized as a function of $M_{org,corr}$ in Fig. 7, including comparisons to the data of previous studies (Table 1). Panel a shows the yield data for $M_{org,corr} < 10\,\mu\text{g m}^{-3}$, corresponding to atmospheric concentrations. Panel b shows the yield data for the full range of $M_{org,corr}$ studied in the laboratory. For $M_{org,corr} < 10\,\mu\text{g m}^{-3}$, the particle phase is dominantly composed of the low-volatility products. Correspondingly, the average carbon oxidation state $\overline{OS_c}$ does not change within the measurement uncerainty. Our analysis, as summarized in discussion of Fig. 5, indicates that the products that partition to the particle phase for $M_{org,corr} < 10\,\mu\text{g m}^{-3}$ are mainly produced by fast reaction pathways that transform first-generation parent compounds into second-generation low-volatility products.

Yield data for $M_{org,corr} > 10\,\mu\text{g m}^{-3}$ are plotted in Fig. 7b. For this range of mass concentration, our analysis concludes that the particle phase is dominantly composed of relatively high-volatility, slow-forming second-generation products. These products are less oxidized (i.e., $-0.4 < \overline{OS_c} < -0.8$). For comparison, Lee et al. (2006a) also carried out experiments for conditions of excess ozone at high $M_{org,corr}$, and the yields reported therein are lower than those of the present study. The difference might be related to the relative humidity of the two studies, which was 40 % in our study and 6 % in Lee et al. (2006a). Winterhalter et al. (2009) showed that increased particle mass yields can be expected for higher relative humidity. Panel b also shows that the yields reported herein are less than those of Griffin et al. (1999). The data reported in Griffin et al. (1999) were for photooxidation experiments, meaning that compared to the ozonolysis results of this study a significant shift to lower volatility might have occurred in the volatility distribution of the products because of additional oxidation by OH.

4   Conclusions

This study investigated the role of second-generation products in the particle mass yield of β-caryophyllene ozonolysis. For concentrations that overlapped with those of

the atmosphere (i.e., 0.1 to 10 µg m^{-3}), the particle mass yield was not sensitive to the ozone concentration. The explanation is that for this range of mass concentration there was a dominant contribution of low-volatility, fast-forming second-generation products to the particle phase. The oxygen-to-carbon elemental ratio of 0.5 indicates

5 that these low-volatility products had 7 to 8 oxygen atoms with estimated vapor pressures of 10^{-12} to 10^{-14} Pa (Li et al., 2011). The data further show that organic particle mass concentration closely correlates with the oxidation state and the material density of the particle-phase organic material. Across the studied range of organic particle mass concentration (0.5–230 µg m^{-3}), the O : C ratio dropped from 0.5 to 0.3, corre-

10 sponding to a decrease in $\overline{OS}_c$ from -0.4 to -0.8. Material density likewise decreased from 1600 to 1300 kg m^{-3}, corresponding to the decrease relative oxygen content.

Prior to the present study, no data points for the particle mass yield of β-caryophyllene ozonolysis had been available in the atmospheric limit of $M_{org} <$ 10 µg m^{-3}. In the absence of data, regional and global chemical transport models

15 have instead employed extrapolations of the data reported by Griffin et al. (1999) to estimate the contribution of sesquiterpene β-caryophyllene oxidation to atmospheric particle mass concentrations (Chung and Seinfeld, 2002; Sakulyanontvittaya et al., 2008b; Zhang and Ying, 2011) (Sect. B and Table S2 of Supplement). Because the data reported by Griffin et al. (1999) were collected at 308 K, estimated enthalpies of

20 vaporization ΔH_{vap} have been used in these literature studies to parameterize yield at 298 K. These parameterizations are represented by the dashed lines in Fig. 7. The yields reported in the present study suggest that Sakulyanontvittaya et al. (2008b), who estimated ΔH_{vap} as approximately 160 kJ mol^{-1}, overestimated the contribution by sesquiterpenes-derived SOM to atmospheric particle mass concentrations. Using

25 an updated ΔH_{vap} of 40 kJ mol^{-1} as well as a material density ρ_{org} of 1300 kg m^{-3} (Bahreini et al., 2005; Offenberg et al., 2006), Carlton et al. (2010) derived the state-of-the-art parameterization that most closely approximates the data set of Griffin et al. (1999). Nevertheless, the comparison between our data set and the parameterization of Carlton et al. (2010) suggests a possible underestimate by that parameterization

Title Page

Abstract | Introduction

Conclusions | References

Tables | Figures

|◄ | ►|

◄ | ►

Back | Close

Full Screen / Esc

Printer-friendly Version

Interactive Discussion

of 100 % to 300 % for organic particle mass concentrations less than $3 \, \mu g \, m^{-3}$.

The ultimate particle mass yield of β-caryophyllene ozonolysis was parameterized for the present study by mass-based stoichiometric yields $\alpha_0 = 0.17 \pm 0.05$, $\alpha_1 = 0.11 \pm 0.17$, and $\alpha_2 = 1.03 \pm 0.30$ for corresponding saturation concentrations of 1, 10, and $100 \, \mu g \, m^{-3}$. Terms α_0 and α_1 had low sensitivity to ozone exposure for the investigated range of conditions whereas term α_2 increased from 0.32 ± 0.13 to 1.03 ± 0.30 as ozone exposure was increased. These findings potentially allow for simplified yet nevertheless accurate parameterizations in air quality and climate models that seek to represent the ozonolysis particle mass yield of certain classes of biogenic compounds.

Supplementary material related to this article is available online at:
http://www.atmos-chem-phys-discuss.net/11/30527/2011/
acpd-11-30527-2011-supplement.pdf.

References

Aiken, A. C., DeCarlo, P. F., and Jimenez, J. L.: Elemental analysis of organic species with electron ionization high-resolution mass spectrometry, Anal. Chem., 79, 8350–8358, doi:10.1021/ac071150w, 2007.

Title Page

Abstract | Introduction

Conclusions | References

Tables | Figures

◄ | ►|

◄ | ►

Back | Close

Full Screen / Esc

Printer-friendly Version

Interactive Discussion

Aiken, A. C., Decarlo, P. F., Kroll, J. H., Worsnop, D. R., Huffman, J. A., Docherty, K. S., Ulbrich, I. M., Mohr, C., Kimmel, J. R., Sueper, D., Sun, Y., Zhang, Q., Trimborn, A., Northway, M., Ziemann, P. J., Canagaratna, M. R., Onasch, T. B., Alfarra, M. R., Prevot, A. S. H., Dommen, J., Duplissy, J., Metzger, A., Baltensperger, U., and Jimenez, J. L.: O/C and OM/OC ratios of primary, secondary, and ambient organic aerosols with high-resolution time-of-flight aerosol mass spectrometry, Environ. Sci. Technol., 42, 4478–4485, doi:10.1021/es703009q, 2008.

Alfarra, M. R., Coe, H., Allan, J. D., Bower, K. N., Boudries, H., Canagaratna, M. R., Jimenez, J. L., Jayne, J. T., Garforth, A. A., Li, S. M., and Worsnop, D. R.: Characterization of urban and rural organic particulate in the lower Fraser valley using two aerodyne aerosol mass spectrometers, Atmos. Environ., 38, 5745–5758, doi:10.1016/j.atmosenv.2004.01.054, 2004.

Atkinson, R., and Arey, J.: Gas-phase tropospheric chemistry of biogenic volatile organic compounds: a review, Atmos. Environ., 37, S197–S219, doi:10.1016/s1352-2310(03)00391-1, 2003.

Bahreini, R., Keywood, M. D., Ng, N. L., Varutbangkul, V., Gao, S., Flagan, R. C., Seinfeld, J. H., Worsnop, D. R., and Jimenez, J. L.: Measurements of secondary organic aerosol from oxidation of cycloalkenes, terpenes, and m-xylene using an aerodyne aerosol mass spectrometer, Environ. Sci. Technol., 39, 5674–5688, doi:10.1021/es048061a, 2005.

Carlton, A. G., Bhave, P. V., Napelenok, S. L., Edney, E. D., Sarwar, G., Pinder, R. W., Pouliot, G. A., and Houyoux, M.: Model representation of secondary organic aerosol in CMAQv4.7, Environ. Sci. Technol., 44, 8553–8560, doi:10.1021/es100636q, 2010.

Chan, A. W. H., Kroll, J. H., Ng, N. L., and Seinfeld, J. H.: Kinetic modeling of secondary organic aerosol formation: effects of particle- and gas-phase reactions of semivolatile products, Atmos. Chem. Phys., 7, 4135–4147, doi:10.5194/acp-7-4135-2007, 2007.

Chan, M. N., Surratt, J. D., Chan, A. W. H., Schilling, K., Offenberg, J. H., Lewandowski, M., Edney, E. O., Kleindienst, T. E., Jaoui, M., Edgerton, E. S., Tanner, R. L., Shaw, S. L., Zheng, M., Knipping, E. M., and Seinfeld, J. H.: Influence of aerosol acidity on the chemical composition of secondary organic aerosol from β-caryophyllene, Atmos. Chem. Phys., 11, 1735–1751, doi:10.5194/acp-11-1735-2011, 2011.

Chen, Q., Liu, Y., Donahue, N. M., Shilling, J. E., and Martin, S. T.: Particle-phase chemistry of secondary organic material: modeled compared to measured O : C and H : C elemental ratios provide constraints, Environ. Sci. Technol., 45, 4763–4770, doi:10.1021/es104398s,

2011.

Chung, S. H. and Seinfeld, J. H.: Global distribution and climate forcing of carbonaceous aerosols, J. Geophys. Res., 107, 4407, doi:10.1029/2001jd001397, 2002.

DeCarlo, P. F., Slowik, J. G., Worsnop, D. R., Davidovits, P., and Jimenez, J. L.: Particle morphology and density characterization by combined mobility and aerodynamic diameter measurements. Part 1: Theory, Aerosol Sci. Technol., 38, 1185–1205, doi:10.1080/027868290903907, 2004.

DeCarlo, P. F., Kimmel, J. R., Trimborn, A., Northway, M. J., Jayne, J. T., Aiken, A. C., Gonin, M., Fuhrer, K., Horvath, T., Docherty, K. S., Worsnop, D. R., and Jimenez, J. L.: Field-deployable, high-resolution, time-of-flight aerosol mass spectrometer, Anal. Chem., 78, 8281–8289, doi:10.1021/ac061249n, 2006.

Donahue, N. M., Robinson, A. L., Stanier, C. O., and Pandis, S. N.: Coupled partitioning, dilution, and chemical aging of semivolatile organics, Environ. Sci. Technol., 40, 02635–02643, doi:10.1021/es052297c, 2006.

Ehara, K., Hagwood, C., and Coakley, K. J.: Novel method to classify aerosol particles according to their mass-to-charge ratio – aerosol particle mass analyser, J. Aerosol Sci., 27, 217–234, 1996.

Fiore, A., Jacob, D. J., Liu, H., Yantosca, R. M., Fairlie, T. D., and Li, Q.: Variability in surface ozone background over the United States: implications for air quality policy, J. Geophys. Res., 108, 4787, doi:10.1029/2003jd003855, 2003.

Fu, P. Q., Kawamura, K., Chen, J., and Barrie, L. A.: Isoprene, monoterpene, and sesquiterpene oxidation products in the high arctic aerosols during late winter to early summer, Environ. Sci. Technol., 43, 4022–4028, doi:10.1021/es803669a, 2009.

Griffin, R. J., Cocker, D. R., Flagan, R. C., and Seinfeld, J. H.: Organic aerosol formation from the oxidation of biogenic hydrocarbons, J. Geophys. Res., 104, 3555–3567, 1999.

Grosjean, D., Williams, E. L., Grosjean, E., Andino, J. M., and Seinfeld, J. H.: Atmospheric oxidation of biogenic hydrocarbons: reaction of ozone with beta-pinene, d-limonene, and trans-caryophyllene, Environ. Sci. Technol., 27, 2754–2758, 1993.

Helmig, D., Balsley, B., Davis, K., Kuck, L. R., Jensen, M., Bognar, J., Smith, T., Arrieta, R. V., Rodriguez, R., and Birks, J. W.: Vertical profiling and determination of landscape fluxes of biogenic nonmethane hydrocarbons within the planetary boundary layer in the Peruvian Amazon, J. Geophys. Res., 103, 25519–25532, doi:25510.21029/25598JD01023, 1998.

Helmig, D., Ortega, J., Duhl, T., Tanner, D., Guenther, A., Harley, P., Wiedinmyer, C., Milford, J.,

and Sakulyanontvittaya, T.: Sesquiterpene emissions from pine trees – identifications, emission rates and flux estimates for the contiguous United States, Environ. Sci. Technol., 41, 1545–1553, doi:10.1021/es0618907, 2007.

Hoffmann, T., Odum, J. R., Bowman, F., Collins, D., Klockow, D., Flagan, R. C., and Seinfeld, J. H.: Formation of organic aerosols from the oxidation of biogenic hydrocarbons, J. Atmos. Chem., 26, 189–222, 1997.

Hu, D., Bian, Q., Li, T. W. Y., Lau, A. K. H., and Yu, J. Z.: Contributions of isoprene, monoterpenes, beta-caryophyllene, and toluene to secondary organic aerosols in Hong Kong during the summer of 2006, J. Geophys. Res., 113, D22206, doi:10.1029/2008jd010437, 2008.

Jaoui, M. and Kamens, R. M.: Gas and particulate products distribution from the photooxidation of α-humulene in the presence of NO$_x$, natural atmospheric air and sunlight, J. Atmos. Chem., 46, 29–54, 2003.

Jaoui, M., Leungsakul, S., and Kamens, R. M.: Gas and particle products distribution from the reaction of β-caryophyllene with ozone, J. Atmos. Chem., 45, 261–287, 2003.

Jaoui, M., Lewandowski, M., Kleindienst, T. E., Offenberg, J. H., and Edney, E. O.: β-caryophyllinic acid: an atmospheric tracer for β-caryophyllene secondary organic aerosol, Geophys. Res. Lett., 34, L05816, doi:10.1029/2006gl028827, 2007.

Kanawati, B., Herrmann, F., Joniec, S., Winterhalter, R., and Moortgat, G. K.: Mass spectrometric characterization of β-caryophyllene ozonolysis products in the aerosol studied using an electrospray triple quadrupole and time-of-flight analyzer hybrid system and density functional theory, Rapid Commun. Mass Sp., 22, 165–186, 2008.

Katrib, Y., Martin, S. T., Rudich, Y., Davidovits, P., Jayne, J. T., and Worsnop, D. R.: Density changes of aerosol particles as a result of chemical reaction, Atmos. Chem. Phys., 5, 275–291, doi:10.5194/acp-5-275-2005, 2005.

King, S. M., Rosenoern, T., Shilling, J. E., Chen, Q., and Martin, S. T.: Cloud condensation nucleus activity of secondary organic aerosol particles mixed with sulfate, Geophys. Res. Lett., 34, L24806, doi:10.1029/2007gl030390, 2007.

King, S. M., Rosenoern, T., Shilling, J. E., Chen, Q., and Martin, S. T.: Increased cloud activation potential of secondary organic aerosol for atmospheric mass loadings, Atmos. Chem. Phys., 9, 2959–2971, doi:10.5194/acp-9-2959-2009, 2009.

Kleindienst, T. E., Smith, D. F., Li, W., Edney, E. O., Driscoll, D. J., Speer, R. E., and Weathers, W. S.: Secondary organic aerosol formation from the oxidation of aromatic hydrocarbons in the presence of dry submicron ammonium sulfate aerosol, Atmos. Environ., 33, 3669–

Particle mass yield from β-caryophyllene ozonolysis

Q. Chen et al.

Title Page

Abstract	Introduction
Conclusions	References
Tables	Figures

◀◀   ▶▶

◀   ▶

Back   Close

Full Screen / Esc

Printer-friendly Version

Interactive Discussion

3681, 1999.

Kleindienst, T. E., Jaoui, M., Lewandowski, M., Offenberg, J. H., Lewis, C. W., Bhave, P. V., and Edney, E. O.: Estimates of the contributions of biogenic and anthropogenic hydrocarbons to secondary organic aerosol at a southeastern US location, Atmos. Environ., 41, 8288–8300, doi:10.1016/j.atmosenv.2007.06.045, 2007.

Knutson, E. O. and Whitby, K. T.: Aerosol classification by electric mobility: apparatus, theory, and applications, J. Aerosol Sci., 6, 443–451, 1975.

Kroll, J. H., Donahue, N. M., Jimenez, J. L., Kessler, S. H., Canagaratna, M. R., Wilson, K. R., Altieri, K. E., R.Mazzoleni, L., Wozniak, A. S., Bluhm, H., Mysak, E. R., Smith, J. D., Kolb, C. E., and Worsnop, D. R.: Carbon oxidation state as a metric for describing the chemistry of atmospheric organic aerosol, Nature Chem., 3, 133–139, doi:10.1038/nchem.948, 2011.

Lee, A., Goldstein, A. H., Keywood, M. D., Gao, S., Varutbangkul, V., Bahreini, R., Ng, N. L., Flagan, R. C., and Seinfeld, J. H.: Gas-phase products and secondary aerosol yields from the ozonolysis of ten different terpenes, J. Geophys. Res., 111, D07302, doi:10.1029/2005jd006437, 2006a.

Lee, A., Goldstein, A. H., Kroll, J. H., Ng, N. L., Varutbangkul, V., Flagan, R. C., and Seinfeld, J. H.: Gas-phase products and secondary aerosol yields from the photooxidation of 16 different terpenes, J. Geophys. Res., 111, D17305, doi:10.1029/2006jd007050, 2006b.

Li, Y. J., Chen, Q., Guzman, M. I., Chan, C. K., and Martin, S. T.: Second-generation products contribute substantially to the particle-phase organic material produced by β-caryophyllene ozonolysis, Atmos. Chem. Phys., 11, 121–132, doi:10.5194/acp-11-121-2011, 2011.

Liu, B. Y. H. and Lee, K. W.: An aerosol generator of high stability, Am. Ind. Hyg. Assoc. J., 36, 861–865, doi:10.1080/0002889758507357, 1975.

Matthew, B. M., Middlebrook, A. M., and Onasch, T. B.: Collection efficiencies in an Aerodyne Aerosol Mass Spectrometer as a function of particle phase for laboratory generated aerosols, Aerosol Sci. Technol., 42, 884–898, doi:10.1080/02786820802356797, 2008.

McMurry, P. H. and Grosjean, D.: Gas and aerosol wall losses in Teflon film smog chambers, Environ. Sci. Technol., 19, 1176–1182, 1985.

McMurry, P. H. and Rader, D. J.: Aerosol wall losses in electrically charged chambers, Aerosol Sci. Technol., 4, 249–268, 1985.

Mensah, A. A., Buchholz, A., Mentel, T. F., Tillmann, R., and Kiendler-Scharr, A.: Aerosol mass spectrometric measurements of stable crystal hydrates of oxalates and inferred relative

Particle mass yield from β-caryophyllene ozonolysis

Q. Chen et al.

ionization efficiency of water, J. Aerosol Sci., 42, 11–19, doi:10.1016/j.jaerosci.2010.10.003, 2011.

Neue, U. D., Kele, M., Bunner, B., Kromidas, A., Dourdeville, T., Mazzeo, J. R., Grumbach, E. S., Serpa, S., Wheat, T. E., Hong, P., and Gilar, M.: Ultra-performance liquid chromatography technology and applications, in: Advances in Chromatography, edited by: Grushka, E. and Grinberg, N., Boca Raton, FL, USA, CRC Press – Taylor & Francis Group, 99–143, 2010.

Ng, N. L., Kroll, J. H., Keywood, M. D., Bahreini, R., Varutbangkul, V., Flagan, R. C., Seinfeld, J. H., Lee, A., and Goldstein, A. H.: Contribution of first- versus second-generation products to secondary organic aerosols formed in the oxidation of biogenic hydrocarbons, Environ. Sci. Technol., 40, 2283–2297, doi:10.1021/es052269u, 2006.

Ng, N. L., Chhabra, P. S., Chan, A. W. H., Surratt, J. D., Kroll, J. H., Kwan, A. J., McCabe, D. C., Wennberg, P. O., Sorooshian, A., Murphy, S. M., Dalleska, N. F., Flagan, R. C., and Seinfeld, J. H.: Effect of NO_x level on secondary organic aerosol (SOA) formation from the photooxidation of terpenes, Atmos. Chem. Phys., 7, 5159–5174, doi:10.5194/acp-7-5159-2007, 2007.

Nguyen, T. L., Winterhalter, R., Moortgat, G., Kanawati, B., Peeters, J., and Vereecken, L.: The gas-phase ozonolysis of β-caryophyllene ($C_{15}H_{24}$). Part II: A theoretical study, Phys. Chem. Chem. Phys., 11, 4173–4183, 2009.

Odum, J. R., Hoffmann, T., Bowman, F., Collins, D., Flagan, R. C., and Seinfeld, J. H.: Gas/particle partitioning and secondary organic aerosol yields, Environ. Sci. Technol., 30, 2580–2585, 1996.

Offenberg, J. H., Kleindienst, T. E., Jaoui, M., Lewandowski, M., and Edney, E. O.: Thermal properties of secondary organic aerosols, Geophys. Res. Lett., 33, L03816, doi:10.1029/2005gl024623, 2006.

Offenberg, J. H., Lewandowski, M., Edney, E. O., Kleindienst, T. E., and Jaoui, M.: Influence of aerosol acidity on the formation of secondary organic aerosol from biogenic precursor hydrocarbons, Environ. Sci. Technol., 43, 7742–7747, doi:10.1021/es901538e, 2009.

Pankow, J. F.: An absorption-model of gas-particle partitioning of organic compounds in the atmosphere, Atmos. Environ., 28, 185–188, 1994a.

Pankow, J. F.: An absorption-model of the gas aerosol partitioning involved in the formation of secondary organic aerosol, Atmos. Environ., 28, 189–193, 1994b.

Pankow, J. F. and Asher, W. E.: SIMPOL.1: a simple group contribution method for predicting vapor pressures and enthalpies of vaporization of multifunctional organic compounds,

Title Page

Abstract	Introduction
Conclusions	References
Tables	Figures

|◄ | ►|

◄ | ►

Back | Close

Full Screen / Esc

Printer-friendly Version

Interactive Discussion

Atmos. Chem. Phys., 8, 2773–2796, doi:10.5194/acp-8-2773-2008, 2008.

Pierce, J. R., Engelhart, G. J., Hildebrandt, L., Weitkamp, E. A., Pathak, R. K., Donahue, N. M., Robinson, A. L., Adams, P. J., and Pandis, S. N.: Constraining particle evolution from wall losses, coagulation, and condensation-evaporation in smog-chamber experiments: optimal estimation based on size distribution measurements, Aerosol Sci. Technol., 42, 1001–1015, doi:10.1080/02786820802389251, 2008.

Presto, A. A. and Donahue, N. M.: Investigation of alpha-pinene plus ozone secondary organic aerosol formation at low total aerosol mass, Environ. Sci. Technol., 40, 3536–3543, doi:10.1021/es052203z, 2006.

Sakulyanontvittaya, T., Duhl, T., Wiedinmyer, C., Helmig, D., Matsunaga, S., Potosnak, M., Milford, J., and Guenther, A.: Monoterpene and sesquiterpene emission estimates for the United States, Environ. Sci. Technol., 42, 1623–1629, doi:10.1021/es702274e, 2008a.

Sakulyanontvittaya, T., Guenther, A., Helmig, D., Milford, J., and Wiedinmyer, C.: Secondary organic aerosol from sesquiterpene and monoterpene emissions in the United States, Environ. Sci. Technol., 42, 8784–8790, doi:10.1021/es800817r, 2008b.

Seinfeld, J. H. and Pankow, J. F.: Organic atmospheric particulate material, Annu. Rev. Phys. Chem., 54, 121–140, doi:10.1146/annurev.physchem.54.011002.103756, 2003.

Seinfeld, J. H., Kleindienst, T. E., Edney, E. O., and Cohen, J. B.: Aerosol growth in a steady-state, continuous flow chamber: application to studies of secondary aerosol formation, Aerosol Sci. Technol., 37, 728–734, doi:10.1080/02786820390214954, 2003.

Shilling, J. E., Chen, Q., King, S. M., Rosenoern, T., Kroll, J. H., Worsnop, D. R., McKinney, K. A., and Martin, S. T.: Particle mass yield in secondary organic aerosol formed by the dark ozonolysis of α-pinene, Atmos. Chem. Phys., 8, 2073–2088, doi:10.5194/acp-8-2073-2008, 2008.

Shilling, J. E., Chen, Q., King, S. M., Rosenoern, T., Kroll, J. H., Worsnop, D. R., DeCarlo, P. F., Aiken, A. C., Sueper, D., Jimenez, J. L., and Martin, S. T.: Loading-dependent elemental composition of α-pinene SOA particles, Atmos. Chem. Phys., 9, 771–782, doi:10.5194/acp-9-771-2009, 2009.

Shu, Y. H. and Atkinson, R.: Atmospheric lifetimes and fates of a series of sesquiterpenes, J. Geophys. Res., 100, 7275–7281, doi:7210.1029/7295JD00368, doi:10.1029/95JD00368, 1995.

Solomon, P., Cowling, E., Hidy, G., and Furiness, C.: Comparison of scientific findings from major ozone field studies in North America and Europe, Atmos. Environ., 34, 1885–1920,

Particle mass yield from β-caryophyllene ozonolysis

Q. Chen et al.

Title Page

Abstract	Introduction
Conclusions	References
Tables	Figures

◄◄ ►►

◄ ►

Back Close

Full Screen / Esc

Printer-friendly Version

Interactive Discussion

2000.

Wang, S. C. and Flagan, R. C.: Scanning electrical mobility spectrometer, J. Aerosol Sci., 20, 1485–1488, doi:10.1016/0021-8502(89)90868-9, 1989.

Winterhalter, R., Herrmann, F., Kanawati, B., Nguyen, T. L., Peeters, J., Vereecken, L., and Moortgat, G. K.: The gas-phase ozonolysis of β-caryophyllene ($C_{15}H_{24}$). Part I: an experimental study, Phys. Chem. Chem. Phys., 11, 4152–4172, doi:10.1039/b817824k, 2009.

Zhang, H. L. and Ying, Q.: Secondary organic aerosol formation and source apportionment in Southeast Texas, Atmos. Environ., 45, 3217–3227, doi:10.1016/j.atmosenv.2011.03.046, 2011.

Particle mass yield from β-caryophyllene ozonolysis

Q. Chen et al.

Title Page

Abstract	Introduction
Conclusions	References
Tables	Figures

|◄   ►|

◄   ►

Back   Close

Full Screen / Esc

Particle mass yield from β-caryophyllene ozonolysis

Q. Chen et al.

Table 1. Compilation of experimental conditions and particle mass yields reported in the literature for β-caryophyllene oxidation.

Reference	[VOC]ᵃ (ppbv)	[O₃] (ppbv)	T (K)	RH (%)	Scavenger for OH or Clᵇ	[NOₓ] (ppbv)	Seed	ρ_{org} (kg m⁻³)ᶜ	ΔM_{org} (µg m⁻³)	Y (%)
Dark ozonolysis at low NOₓ										
Grosjean et al. (1993)	540	80	–	–	Cyclohexane	< 1	None	–	–	12
Jaoui et al. (2003)	601	640	287–290	80–85	None	< MDLᵈ	None	–	–	62ᵉ
Lee et al. (2006a)	88	> 350	293	6	Cyclohexane	< 5	ASᶠ	1250	336	45
Winterhalter et al. (2009)	305–331	200	296	Dry	HCOOH	–	None	1000	310–660	19–41
	239–315	100–200	296	Dry	HCHO	–	None	1000	130–180	9–12
	258–566	100–200	296	Dry	None	–	None	1000	50–370	6–24
	295–296	200	296	36	None	–	None	1000	420–440	27–28
This studyᵍ	1–46	50–200ʰ	298	40	Cyclohexane	< 1	AS	1200–1600	0.5–230	8–70
Photooxidation										
Huffmann et al. (1997)	100–102	–	316–322	–	None	268–283	AS	1000	845–998	103–125
Griffin et al. (1999)	6–13	–	307–309	–	None	24–54	AS	1000	18–82ⁱ	37–79
Lee et al. (2006b)	37	–	295	56	None	25–40	None	1250	212	68

[a] The reacted VOC concentration depends on ozone or OH concentration.
[b] Criegee intermediate.
[c] The SOM densities are measured values in this study and assumed values in other studies.
[d] Minimum detection limit of the NOₓ analyzer (Thermo 8440E).
[e] Calculated from the reported carbon yield of 39 % by applying an OM : OC ratio of 1.6.
[f] Dry ammonium sulfate particles.
[g] Other results are reported in Li et al. (2011) and Chen et al. (2011).
[h] Steady-state concentrations (i.e., excess ozone concentrations).
[i] Particle measurements were conducted outside the reactor at 298 K.

Table 2. Experimental conditions and results for the dark ozonolysis of β-caryophyllene. The terms ΔVOC, $(M_{org})_{outflow}$, $M_{org,corr}$, and $\overline{OS_c}$, respectively represent the reacted concentration of the precursor VOC in an experiment, the mass concentration of particle-phase SOM measured by the AMS, the mass concentration of particle-phase SOM corrected by wall loss and used in the yield calculation (Eq. 1), and the average oxidation state of carbon for particle-phase SOM, calculated as $2(O:C) - 1(H:C)$ (Kroll et al., 2011). The $O:C$ and $H:C$ ratios were originally reported in Chen et al. (2011). Material density ρ_{org} is reported only for experiments using monodisperse seed and having $(M_{org})_{outflow} > 1\,\mu g\,m^{-3}$. For Exp. #10, a ^{210}Po charger was installed in the seed injection line, which neutralized the charged particles exiting the DMA and prior to entering the chamber. As a result of neutralization, electrostatic particle loss to the bag walls decreased (McMurry and Rader, 1985).

| Exp. No	Date	Reaction conditions			Measured quantities at steady state				Derived quantities					
		Seed diameter $d_{m,+1}$ (nm)	ΔVOC (ppbv)	$[O_3]_{ss}$ (ppbv)	$(M_{org})_{outflow}$ ($\mu g\,m^{-3}$)	O:C	H:C	N:C	ρ_{org} (AMS-SMPS) ($kg\,m^{-3}$)	OM:OC	$\overline{OS_c}$	β (h^{-1})	$M_{org,corr}$ ($\mu g\,m^{-3}$)	Y (%)
1	3 Apr 2009	68.5	1.6	50	0.4±0.0	0.49	1.51	0.036	–	1.82	−0.54	1.04±0.11	1.8±0.2	13.2±1.2%
2	12 Apr 2009	68.5	3.1	50	1.1±0.0	0.49	1.49	0.013	1810±190	1.79	−0.51	1.04±0.11	5.3±0.4	20.4±1.7%
3	17 Apr 2009	68.5	6.3	50	3.4±0.1	0.45	1.48	0.007	1450±110	1.73	−0.58	1.04±0.11	15.8±1.4	30.1±2.7%
4	18 Apr 2009	68.5	6.4	100	4.3±0.3	0.45	1.49	0.006	1400±130	1.73	−0.59	1.04±0.11	20.0±2.0	37.4±3.8%
5	20 Apr 2009	68.5	6.5	200	6.3±0.2	0.43	1.49	0.006	1520±90	1.71	−0.62	1.04±0.11	29.6±2.6	54.8±4.9%
6	23 Apr 2009	68.5	12.9	50	9.3±0.4	0.40	1.48	0.003	1330±60	1.66	−0.69	1.04±0.11	44.4±4.1	41.3±3.8%
7	26 Apr 2009	68.5	13.2	200	15.9±0.3	0.36	1.49	0.003	1300±70	1.61	−0.77	1.04±0.11	75.8±6.5	68.7±5.9%
8	6 May 2009	49.5	0.8	50	0.1±0.0	0.53	1.57	0.052	–	1.90	−0.51	1.04±0.11	0.5±0.1	8.0±1.0%
9	7 May 2009	49.5	1.6	50	0.4±0.0	0.53	1.52	0.029	–	1.87	−0.46	1.04±0.11	1.7±0.2	13.0±1.2%
10	8 May 2009	49.5	1.6	100	0.9±0.0	0.51	1.49	0.024	–	1.83	−0.47	0.49±0.03	2.5±0.1	18.6±0.9%
11	9 May 2009	49.5	1.6	200	0.4±0.0	0.53	1.51	0.025	–	1.86	−0.45	1.04±0.11	1.9±0.2	14.6±1.7%
12	12 May 2009	49.5	3.2	50	0.8±0.0	0.53	1.51	0.015	–	1.85	−0.46	1.04±0.11	3.7±0.3	13.6±1.2%
13	14 May 2009	49.5	3.3	100	0.9±0.0	0.53	1.50	0.012	–	1.85	−0.43	1.04±0.11	4.5±0.4	16.3±1.4%
14	15 May 2009	49.5	3.3	200	1.3±0.0	0.53	1.50	0.011	1520±100	1.85	−0.44	1.04±0.11	6.1±0.5	21.9±2.0%
15	17 May 2009	49.5	6.4	50	3.2±0.0	0.50	1.48	0.006	1430±140	1.80	−0.48	1.04±0.11	15.2±1.3	28.4±2.4%
16	19 May 2009	49.5	6.5	100	4.2±0.1	0.49	1.49	0.006	1400±110	1.79	−0.50	1.04±0.11	19.9±1.7	36.6±3.1%
17	20 May 2009	49.5	6.6	200	5.3±0.2	0.48	1.49	0.005	1370±100	1.77	−0.53	1.04±0.11	25.3±2.3	46.1±4.2%
18	23 May 2009	49.5	12.8	50	9.3±0.2	0.42	1.48	0.004	1360±70	1.69	−0.65	1.04±0.11	44.4±3.8	41.4±3.6%
19	26 May 2009	49.5	13.1	100	10.8±0.1	0.39	1.48	0.003	1330±60	1.65	−0.69	1.04±0.11	51.4±4.3	47.2±4.0%
20	29 May 2009	49.5	13.4	200	16.1±0.4	0.37	1.48	0.002	1340±80	1.62	−0.75	1.04±0.11	77.4±6.8	69.5±6.1%
21	4 Jun 2009	49.5	1.6	50	0.4±0.0	0.53	1.52	0.021	–	1.85	−0.46	1.04±0.11	1.8±0.2	13.4±1.2%
22	5 Jun 2009	49.5	1.7	200	0.6±0.0	0.53	1.51	0.016	–	1.85	−0.45	1.04±0.11	2.8±0.3	20.3±1.8%
23	7 Jun 2009	49.5	1.6	100	0.5±0.0	0.54	1.51	0.017	–	1.89	−0.39	1.04±0.11	2.1±0.2	15.8±1.4%
24	12 Jun 2009	poly	45.7	100	47.7±0.5	0.33	1.48	0.002	–	1.56	−0.82	1.04±0.11	227.1±19.2	59.6±5.0%
25	17 Jun 2009	49.5	13.0	100	8.4±0.2	0.41	1.48	0.002	1260±50	1.68	−0.66	1.04±0.11	40.0±3.5	36.8±3.2%
26	18 Jun 2009	poly	44.9	50	36.3±1.7	0.33	1.47	0.003	–	1.57	−0.81	1.04±0.11	172.6±16.6	46.0±4.4%
27	14 Sep 2010	46.1	13.0	50	18.2±0.2	0.35	1.47	0.003	1230±60	1.57	−0.77	0.19±0.02	30.7±1.3	28.7±1.3%
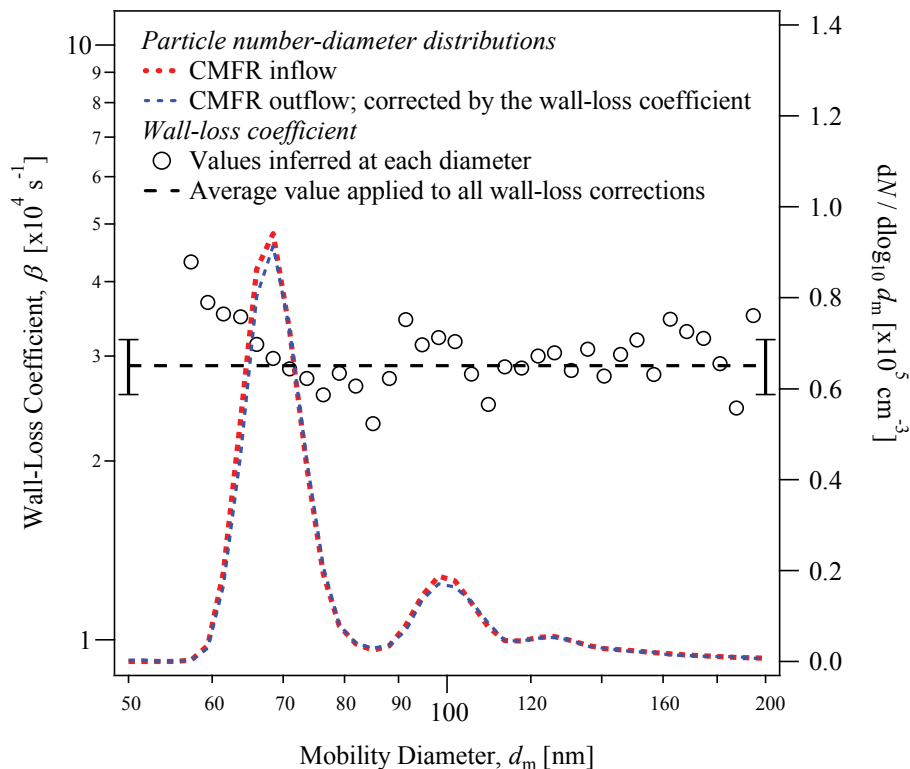
Fig. 1. Measurement of particle wall-loss coefficients β (s^{-1}) in the Harvard Environmental Chamber. Data are shown for one experiment using a population of dry ammonium sulfate particles. Points show the wall-loss coefficient inferred at each diameter such that the outflow number-diameter distribution matches the inflow distribution. No trend with particle diameter is apparent. Therefore, wall losses are accurately represented by an average value, shown as dotted line, for the investigated particle population. The error bars represent one-sigma standard deviation of three replicate experiments.
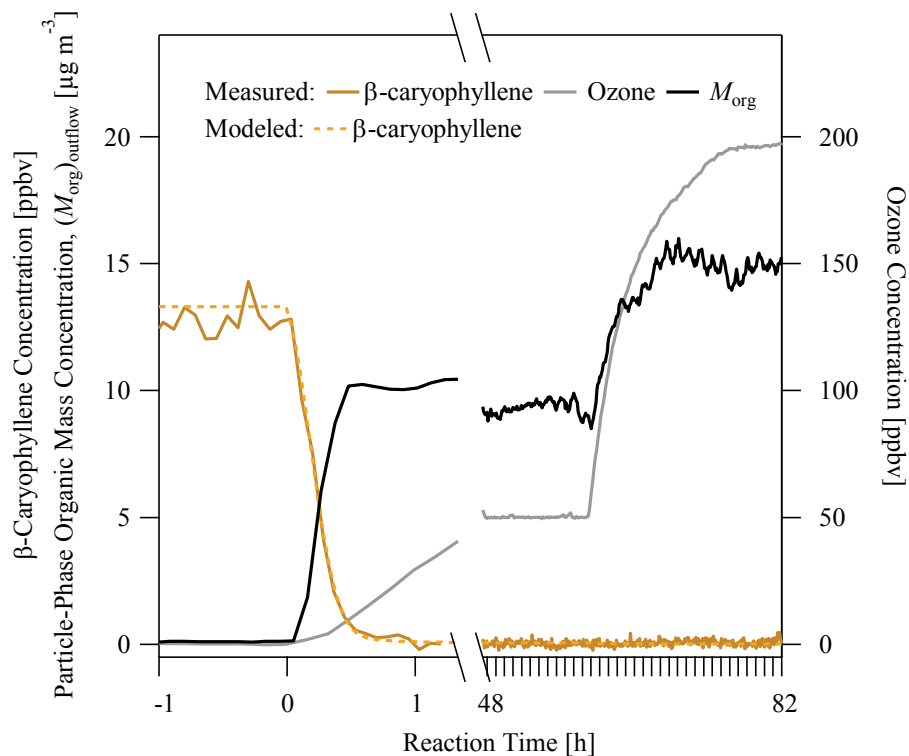
Fig. 2. A typical time series for the transient phase of the CMFR showing the loss of β-caryophyllene, the appearance of particle-phase secondary organic material following the introduction of ozone, and the increase of particle-phase organic material following the elevation of ozone concentration.

Title Page

Abstract | Introduction

Conclusions | References

Tables | Figures

|◄ | ►|

◄ | ►

Back | Close
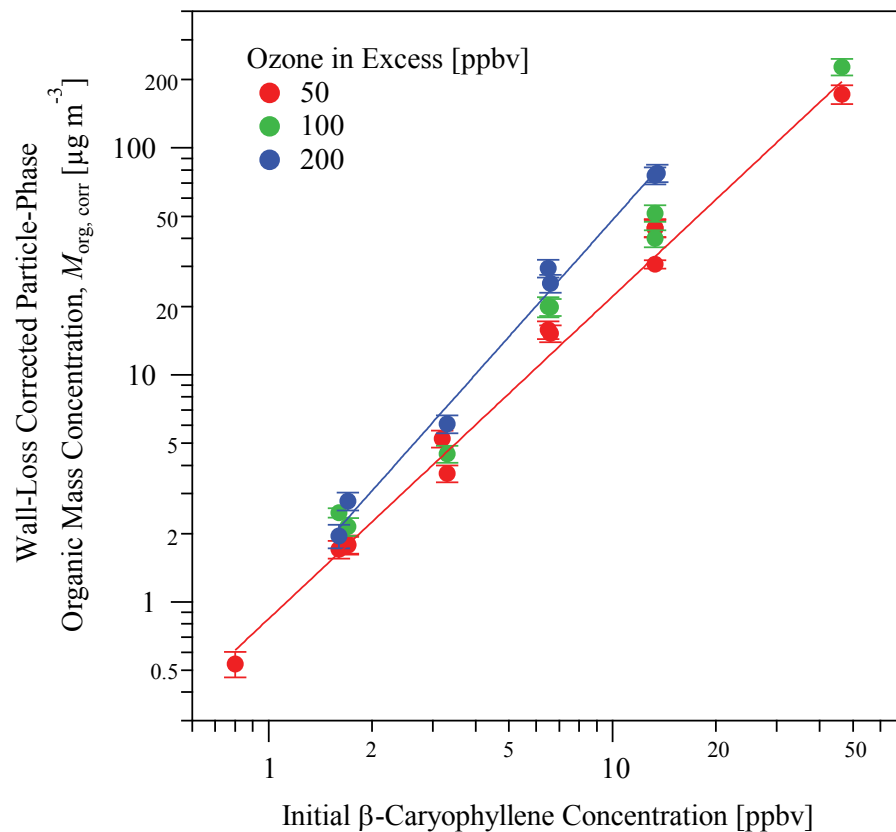
Full Screen / Esc

Printer-friendly Version

Interactive Discussion

Fig. 3. Organic particle mass concentrations at steady state in the CMFR for increasing initial concentration of β-caryophyllene and three different ozone concentrations. The plotted concentrations are corrected for wall loss (Eq. 1). Uncertainties shown for the data points represent the propagated standard deviation (one sigma) of both the temporal variation of M_{org} as well as the wall-loss corrections. Lines are shown to guide the eye.
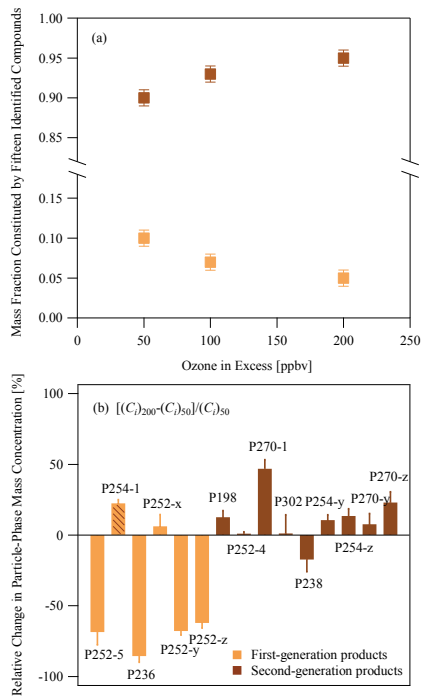
Fig. 4. (a) Mass fractions of first- and second-generation products for increasing ozone concentration. The ordinate of mass fraction represents the sum of the mass concentrations of either the first- or second-generation products divided by the combined sum of first- and second-generation mass concentrations, all measured by UPLC-ESI-ToF-MS for filter-extracted samples (Li et al., 2011). **(b)** The percent change in mass concentration at 50 compared to 200 ppbv O_3 for the fifteen identified products. Experiments in this figure are for 13 ppbv of reacted β-caryophyllene. Error bars represent the one-sigma standard deviation of three replicate experiments. P254-1 is hashed because the data of the present study suggest that this product might have been assigned incorrectly in previous work as a first-generation product (Li et al., 2011); it can instead be assigned as a second-generation product (see main text).

Full Screen / Esc

Printer-friendly Version

Interactive Discussion

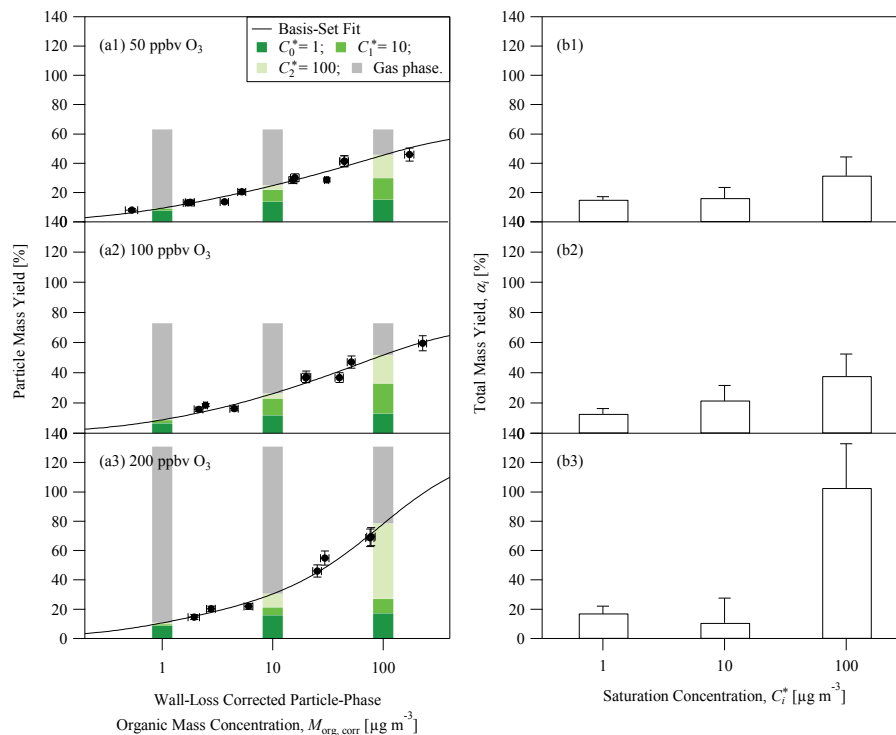**Fig. 5. (a1–a3)** Particle mass yield and basis-set parameterization for the dark ozonolysis of β-caryophyllene. **(b1–b3)** Optimized parameter α_i for product classes of $C_i^* = \{1, 10, 100\}$ µg m^{-3}. Data are shown for 50, 100, and 200 ppbv ozone.
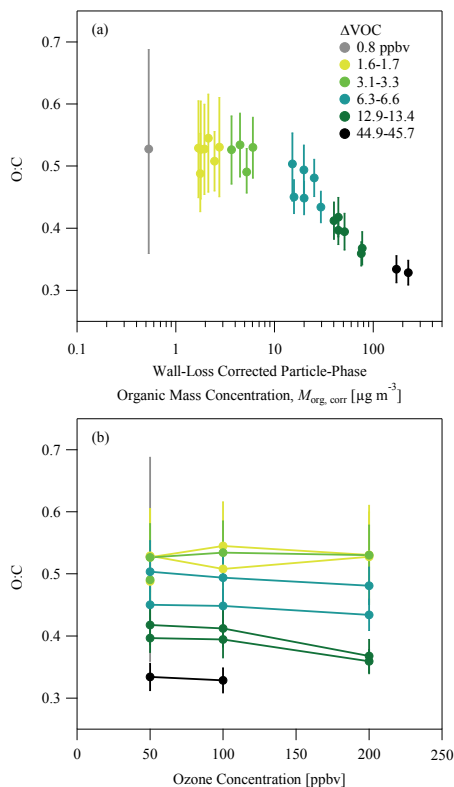
Fig. 6. Oxygen-to-carbon elemental ratios of particle-phase SOM produced by β-caryophyllene ozonolysis for **(a)** increasing particle-phase organic mass concentration and **(b)** increasing ozone concentration. The elemental ratios were determined from the particle-phase high-resolution mass spectra (Aiken et al., 2007, 2008; Chen et al., 2011). Error bars represent the one-sigma measurement precision (Chen et al., 2011). Data are colored by the reacted concentration of β-caryophyllene.
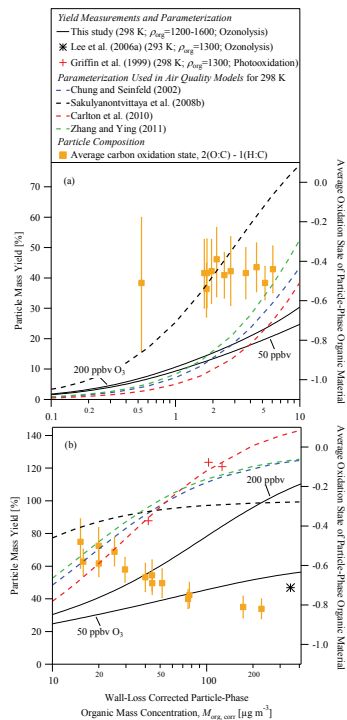
Fig. 7. Comparison of particle mass yields parameterized in this study to those reported in the literature for β-caryophyllene oxidation. **(a)** Data are shown for the atmospherically relevant range of organic particle mass concentration (0.1–$10\,\mu g\,m^{-3}$). **(b)** Data are shown over an extended range of organic particle mass concentration (10–$400\,\mu g\,m^{-3}$). A material density ρ_{org} of $1300\,kg\,m^{-3}$ was assumed to convert the volume-based data sets of Lee et al. (2006a) and Griffin et al. (1999) to mass-based data sets. This density corresponded to $M_{org,corr} > 10\,\mu g\,m^{-3}$ of the present study (Fig. S3). A vaporization enthalpy of $40\,kJ\,mol^{-1}$ was used for temperature compensation from 308 to 298 K for the data reported by Griffin et al. (1999). The dashed lines show four different parameterizations that have been used in air quality and climate models for estimating sesquiterpene-derived particle mass concentrations (Sect. B of Supplement). The average carbon oxidation state of the particle-phase SOM is also represented in the figure (orange squares). Error bars for the oxidation state are derived by propagating the one-sigma measurement precision of the O : C and H : C ratios (Chen et al., 2011).